Supporting Information

Bárcena *et al*. 10.1073/pnas.0805270106

SI Text

Shape of CoV Particles. Although most of the particles in our preparations had a clear spherical shape, a minor proportion of the population (≈7% for MHV) showed some degree of ellipticity. However, in most cases, the deviation from a spherical shape was almost negligible, with axial ratios less than 1.2. The 3D nature of our data allowed us to look at the relative position in the ice layer of the most elliptical particles, showing that they occurred at a higher level than the spherical particles, and therefore, closer to the water-air interface (Fig. S1). This observation strongly suggests that the ellipticity observed could be a result of distortions induced by this proximity. Consequently, all of the elliptical particles were discarded from subsequent analysis.

Centering of Coronavirion Particles, Size Determination, and Measurement of Envelope Thickness. The diameter of the viral envelope was measured from averaged radial density profiles of top-view projections. The spherical shape of most MHVs and TGEVs allows for this rotational averaging, which greatly enhances the overall signal, provided that the center of the particle is correctly assigned. An automatic procedure to ascertain both the particle center and the envelope radius was designed. For the whole process, the contrast of the reconstructions was reversed.

The first part of the procedure consisted of obtaining an estimate of the virion size. To this end, the top view projection for each virus particle was generated, band-pass filtered, and rotationally averaged. The radial intensities of the resulting image were plotted and the envelope radius was considered to equal the external value at which the intensity becomes zero. It should be noted that the background intensity in our tomograms approximates zero as a result of the normalization applied before reconstruction, which consists of subtracting and dividing each image in the tilt series by its average intensity. This normalization additionally corrects for the differences in illumination in the tilt series collection.

The second part of the procedure addressed the centering of the viruses. A spherical mask, 25 pixels larger in radius than the measured size, was applied to the volumes. The top view projection was cross-correlated with its rotationally averaged image, providing the initial XY shifts needed to center the virus particle. The Z-shift was obtained by cross-correlation of the side-view projection of the volume with a band-pass filtered centered circle of the size of the virus. When the shifts were applied to the volume, the whole process was iterated until convergence to refine both the size and the centering of the particle (for an outline of the entire procedure, see Fig. S4).

In the final rotationally averaged density profiles, the region corresponding to the envelope, which shows two peaks in the best reconstructions, is clearly distinguishable from the rest. The slope of the curve was computed for this part of the density profile. The envelope thickness was considered to be the distance between the external and internal radii of maximum slope.

Cryo-Electron Microscopy of CoVs and DOPC Liposomes. To assist in the interpretation of the bilaminar profile of the envelope observed in the tomograms, we collected and analyzed cryo-electron focal pair images of MHV, TGEV, and DOPC liposomes.

Suspensions of DOPC liposomes and cryo-electron microscopy grids carrying these liposomes were prepared as described before (1). Samples were examined by EM by using the same experimental set-up as for tomography data collection. Focal pairs of MHV particles and DOPC liposomes were collected at 1 and 4 μm, 2 and 4 μm, and 2 and 8 μm underfocus using a semi-automatic program for data collection (2). For TGEV, focal pairs at 2 and 4 μm underfocus were acquired. The nominal magnification was ×34,000, which resulted in a pixel size at the specimen level of 0.38 nm. The dose per image was 25 e$^-$/Å^2. CoV and DOPC particles were extracted from the images and processed according to an analogous iterative procedure to the one used for the CoV tomograms. Being 2D images, the problem of centering the particles was reduced in this case to finding the XY shifts, which was achieved by cross-correlation of the images with the band-pass filtered rotationally averaged image of the particle. The thickness of the MHV envelopes and of DOPC lipid bi-layers was measured in the rotationally averaged density profiles as described for the CoV particle reconstructions.

Fig. S2 shows focal pairs of a DOPC liposome (Fig. S2*A*) and a TGEV virus particle (Fig. S2*B*), together with the corresponding density profiles, to allow a direct comparison with the results obtained for MHV (Fig. 4*C* in main text).

Three-Dimensional Analysis of MHV Envelope. Striations in the virion envelope, often at what seemed to be relatively regular distances, were observed in XY sections of the tomograms. This abundant feature is attributable to the M protein, as its occurrence is unrelated to that of the spike protein and the other integral envelope protein, E, is only a minor and small component of the virus envelope. To gain a deeper insight into the organization of the M striations in the envelope, we investigated their distribution in 3D by image analysis of 10 MHV particles of different sizes obtained from different tilt series.

First, the densities of the 3D-centered virus particles were radially averaged over the width of the envelope and their contrast was reversed. In this way, radially oriented striations become maxima in the averaged density maps. Although no directly interpretable lattice (e.g., hexagonal forms) was apparent, local clusters were found for which these maxima seemed to be spaced by some preferred distance (Fig. S3*A*).

To investigate possible regularities and whether the distribution of maxima deviated significantly from a random distribution, image analysis of each individual envelope proceeded via the following steps: (*i*) determination of the position of the maxima on the radially averaged envelope, i.e., on a spherical shell; (*ii*) calculation of all inter-maxima distances; (*iii*) normalization of the obtained distance distribution to account for the spherical geometry of the envelope; and (*iv*) comparison with the data obtained from 250 simulations of the same number of randomly distributed points as maxima found in the envelope.

The first step combined an automatic peak-determination procedure (based on the relative contrast and intensity) with manual assessment and refinement of every peak. The manual step showed to be important to correct for effects of the missing wedge (e.g., anisotropy of the signal, directional smearing of densities), to which the automatic procedure is blind.

The normalization step is required because the probability of finding two randomly distributed points on a sphere scales with their distance. For example, if the first point defines one pole of a sphere, the chance of encountering a second (randomly placed) point is largest at the equator and virtually zero at the opposite pole. In short, the relative occurrence F of distances within a given interval $d \in [d_i, d)_j$ is given by:

$$F_d = f_d/g_d$$

where f_d denotes the fraction of distances found within the interval d, while g_d denotes the probability in d for randomly distributed points. The function g_d is given by:

$$g_d = \frac{1}{2}\left(\cos\left(\frac{d_i}{R}\right) - \cos\left(\frac{d_j}{R}\right)\right)$$

for a spherical shell, i.e., the viral envelope, of radius R. The inter-striation distance distribution is normalized such that 1 is the expectancy value for a random distribution.

The results of this analysis are depicted in Fig. S3 *B* and *C*. For all of the individual virions, we found a peak at approximately 6.5 nm distance that differed significantly from a random distribution (Fig. S3*B*), and which was also distinct when the results of the 10 MHV particles were combined to reduce the background noise (Fig. S3*C*). A clear peak at approximately twice this distance cannot be unambiguously identified. This is to be expected from our analysis and correlates with the observation of local and relatively loosely arranged striation patches on the spherical envelope.

1. Stuart MC, Boekema EJ (2007) Two distinct mechanisms of vesicle-to-micelle and micelle-to-vesicle transition are mediated by the packing parameter of phospholipid-detergent systems. *Biochim Biophys Acta* 1768:2681–2689.

2. Oostergetel GT, Keegstra W, Brisson A (1998) Automation of specimen selection and data acquisition for protein electron crystallography. *Ultramicroscopy* 74:47–59.
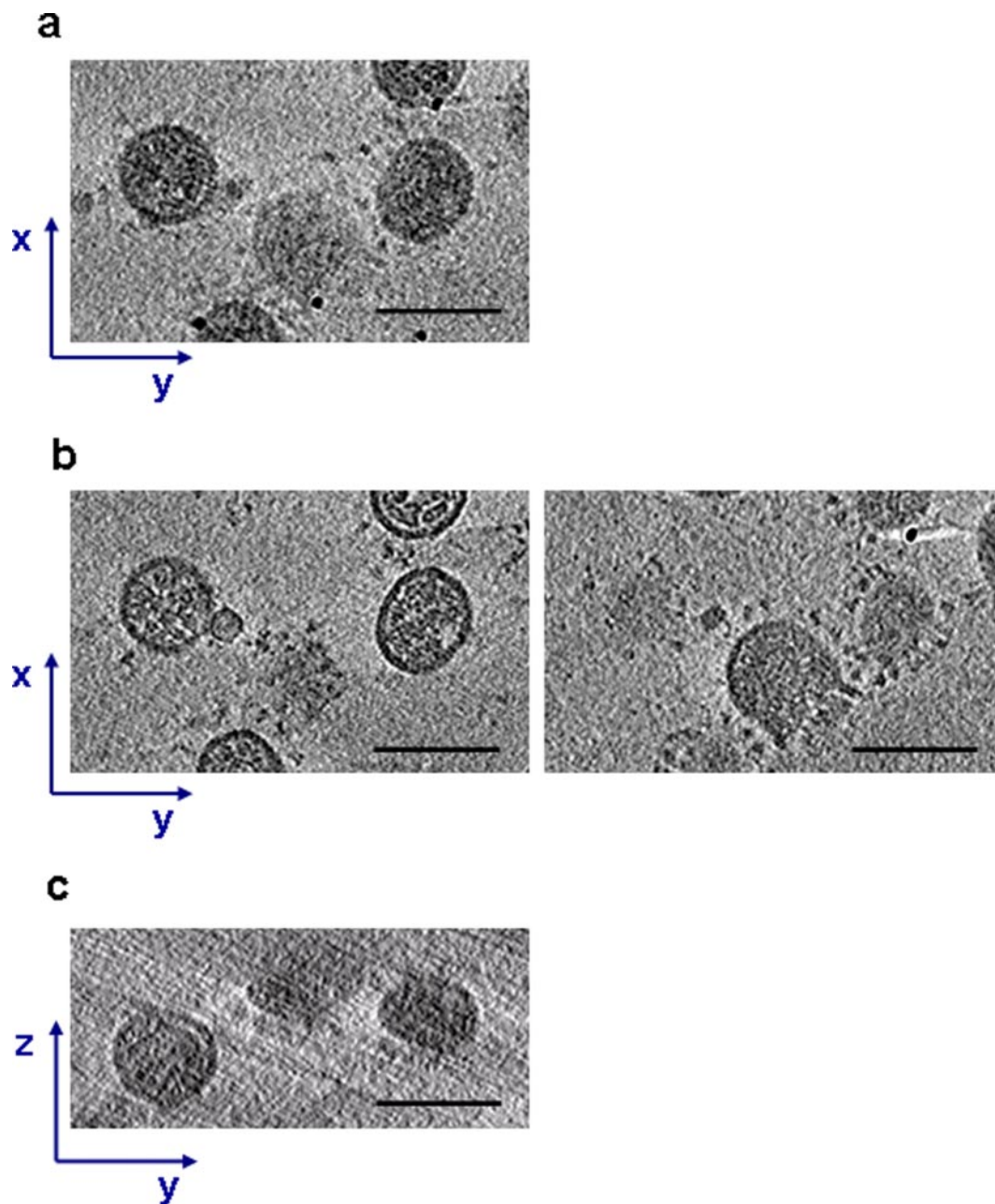
Fig. S1. Occurrence of elliptical MHV particles. (*a*) An XY projection of part of the tomogram (averaging of 80 nm), which would resemble the aspect of the preparation observed by 2D microscopy. The image shows what, in projection, appears as a possibly spherical MHV particle (*Left*), a disrupted virion (*Middle*), and an elliptical MHV particle (*Right*). (*b*) XY sections through the tomogram details of these virions (17 nm thick and 23 nm apart) show that the 3 virions lay at different heights in the ice layer. This becomes more apparent when directly examining the Z dimension: (*c*) ZY projection (130 nm averaged) of the area shown in *a* and *b*. The limit of the ice layer is not visible per se in this image, because of its low intrinsic contrast, although it is suggested by the profile in the ZY projection of the disrupted virion (particle, *Middle*). The correlation between the relative MHV particle heights and their shape/preservation suggests that proximity of the water-air interface induces a flattening that gives MHV particles an elliptical appearance. Closer proximity seems to even cause disruption of the virions. (Scale bars, 100 nm.)
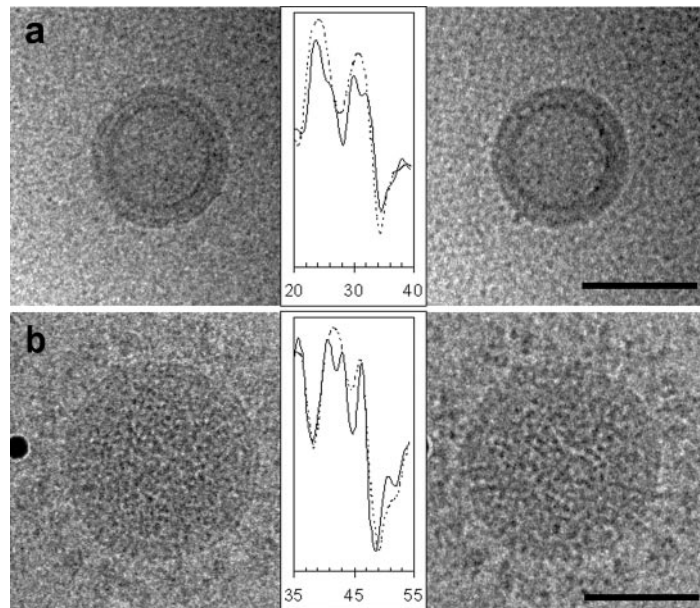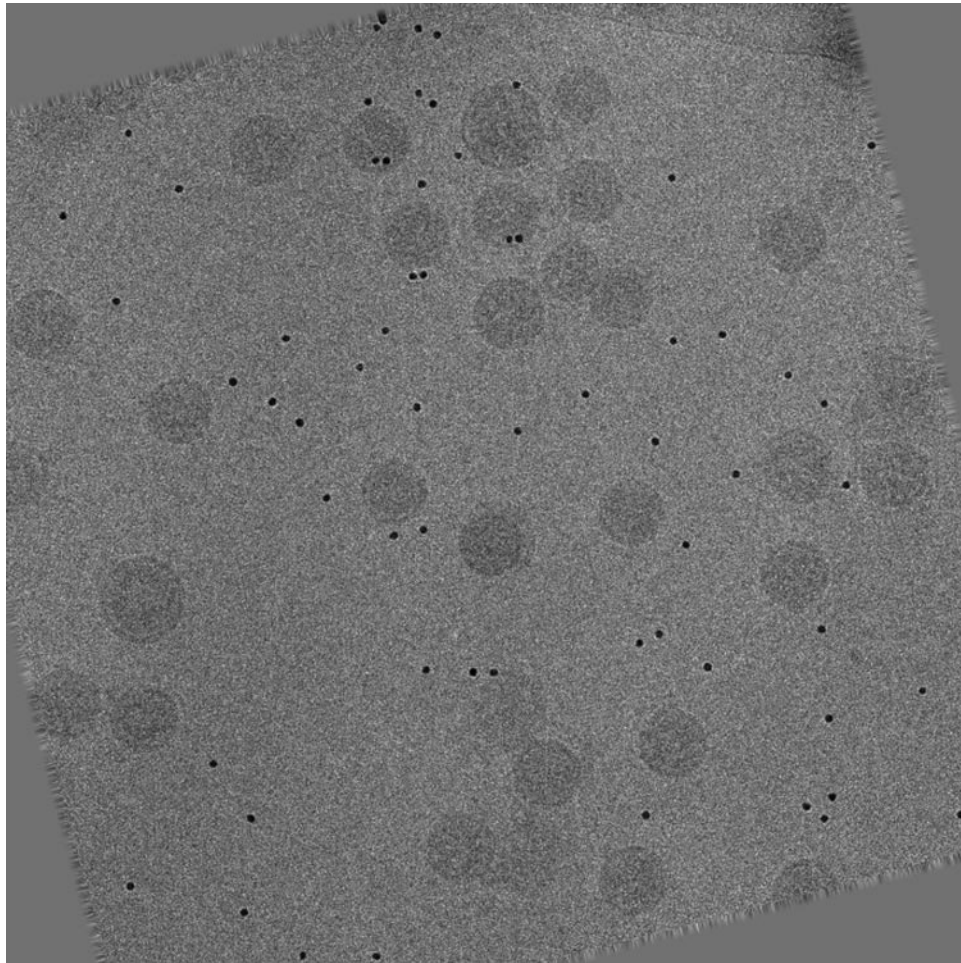
Fig. S2. Focal pairs and radial density profiles of (*a*) a bilamellar liposome and (*b*) a TGEV virion. In the case of the liposome, at 2 μm underfocus (*Left*, continuous plot) the two bi-layers show a bilaminar appearance, whereas at 4 μm underfocus, (*Right*, dotted plot) the two peaks of each bilayer are not resolved and merge into one. In contrast, but equivalently to MHV, the TGEV envelope shows a trilaminar profile at 2 μm underfocus, indicating the presence of a third lamina additional to the lipid bilayer. The triple-layered TGEV envelope is not resolved at 4 μm underfocus (used for tomography), yielding an envelope with a bilaminar appearance. Note that the width of the peaks, indicative of the thickness observed in the images, does not change with the defocus. All measurements are in nanometers. (Scale bar, 50 nm.)
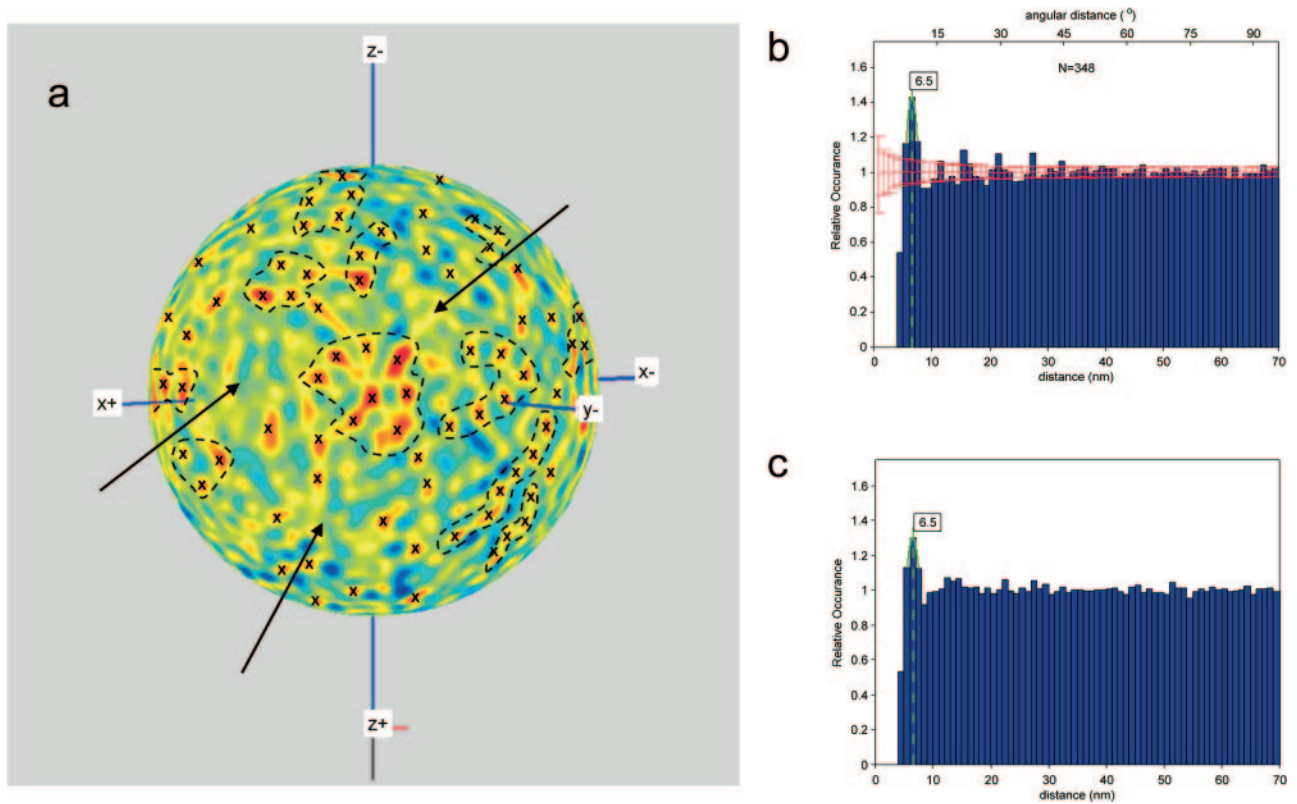
Fig. S3. (*a*) Radial projections of the envelope densities of one of the MHV virions. On the sphere, red represents higher density values; blue, lower densities. The selected maxima are indicated with crosses. Patches of similarly separated maxima (some of which are roughly delineated on the sphere) alternate with areas without distinct peaks (arrows). The axes indicate the original orientation of the tomographic reconstruction. (*b*) Relative occurrence of distances between maxima for the envelope shown in *a* with respect to the expectation value of a random distribution. The average of 250 simulations of randomly distributed points is shown in red with SDs depicted by error bars. (*c*) Relative occurrence of distances between striations for a total of 10 MHV virions. The green lines in *c* and *d* show the parabolic fit to the strongest peak with the distance value in the text box.

Fig. S4. Flow diagram of the process followed to center the cryo-tomograms of CoV particles in 3D and to measure the diameter of the virion envelope (see text for details).
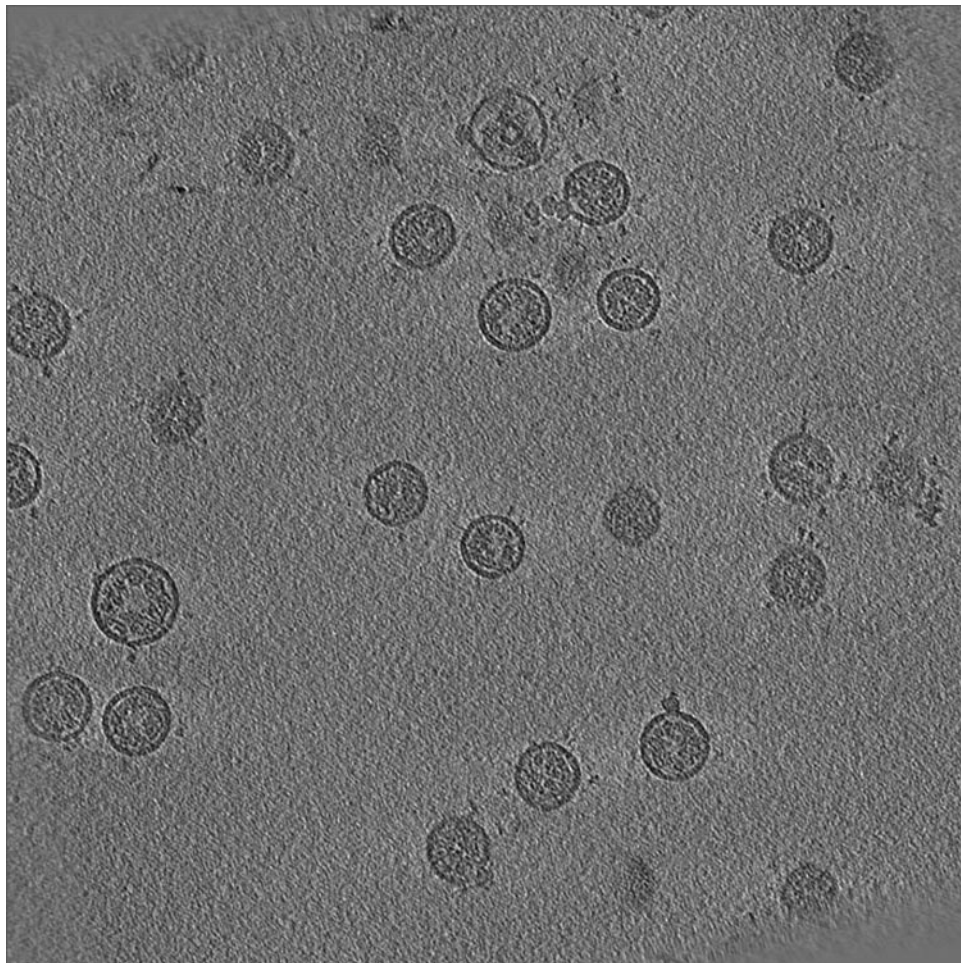
Movie S1.   Aligned tilt series of one of the examined fields of purified MHV particles. To assist in the visualization of the otherwise very noisy images, the images of the tilt series have been low-pass filtered to 5.8 nm.
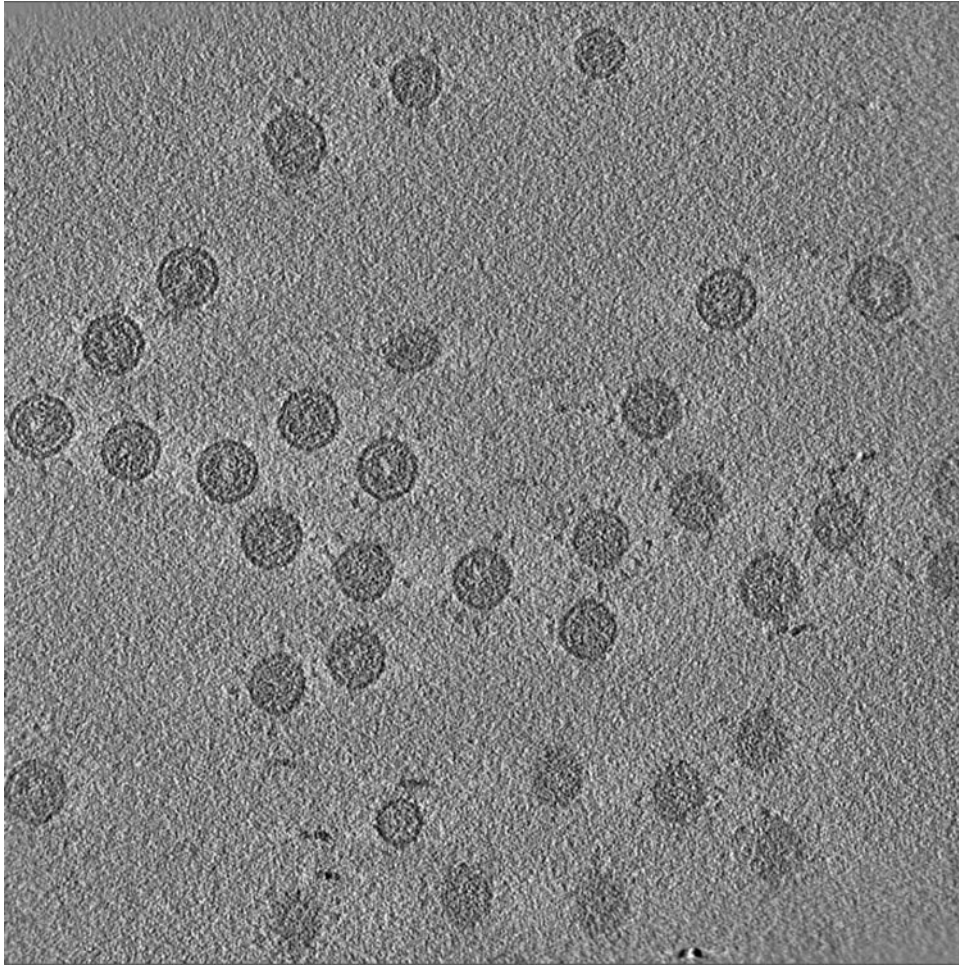
Movie S1 (MOV)

Movie S2. Tomographic reconstruction of purified MHV particles. The tomogram shown here was generated from the filtered tilt series shown in Movie S1. The slices through the tomogram are 1.74 nm thick.

Movie S2 (MOV)

Movie S3.   Cryo-electron tomography of purified TGEV particles. Note that the only elliptical particle is at a different height that the surrounding spherical TGEV virions. The tomogram shown here was generated in an analogous manner to that in Movie S2. The slices through the tomogram are 1.74 nm thick.

Movie S3 (MOV)